

UNIVERSIDADE DE SÃO PAULO

INSTITUTO DE FÍSICA  
CAIXA POSTAL 20516  
01498-970 SÃO PAULO - SP  
BRASIL

# PUBLICAÇÕES

IFUSP/P-1067

**THERMALIZATION RELATED EFFECTS IN THE  
ELECTROFISSION OF PRACTINIDE NUCLEI**

**J.D.T. Arruda-Neto, T. Saito, M. Sugawara,  
T. Tamae, H. Miyase, K. Abe, K. Takahisa,  
O. Konno, and M. Oikawa**

Laboratory of Nuclear Science  
Tohoku University, Sendai, Japan

**S. Simionatto**

Instituto de Física, Universidade de São Paulo

Julho/1993

# THERMALIZATION RELATED EFFECTS IN THE ELECTROFISSION OF PREACTINIDE NUCLEI

J.D.T. Arruda-Neto\*, T. Saito, M. Sugawara, T. Tamae, H. Miyase,  
K. Abe, K. Takahisa, O. Konno, and M. Oikawa

Laboratory of Nuclear Science, Tohoku University, Sendai, Japan

S. Simionatto

Physics Institute, University of São Paulo, São Paulo, Brazil

## ABSTRACT

The absolute electrofission cross section of Au and Ta was measured in the energy interval 40–250 MeV. Pronounced inflexions of the  $(e, f)$  curves are observed for both Au and Ta around 200–220 MeV, which are signatures of structures in the corresponding photofission cross-section curves. We show that these  $(\gamma, f)$  structures are originated in the stage of preequilibrium emissions in the nuclear thermalization process. The question associated to a possible connection between thermalization effects and competing photoexcitation mechanisms is addressed.

*Keyword abstract:*

[NUCLEAR REACTION: Au, Ta( $e, f$ ), 40–250 MeV. Measured  $\sigma(e, f)$ ; deduced photofission cross section. Thermalization process studied.]

PACS:

24.75.+i, 25.85.Jg, 27.80.+w

\*Permanent Address: Physics Institute, University of São Paulo, São Paulo, Brazil.

## I. INTRODUCTION

Photonuclear reactions (induced by real or virtual photons) are very suitable to probe the nuclear and nucleonic structure, for the reaction mechanism is well understood comparatively to the nucleon-nucleon interactions.

For photon energies above the photopion production threshold ( $\sim 140$  MeV), in particular, pion production is the dominant process responsible for photoabsorption. At these energies, the absorption of a photon initiates an intranuclear cascade (the fast step, with a duration  $\tau_0 < 10^{-22}$  s) in which particles of the continuum leave the nucleus (preequilibrium emission) all along until equilibration (compound nucleus formation); as pointed out before<sup>1,2)</sup>, in this system the thermodynamic equilibrium is reached very quickly, during a time  $\tau_{eq} > (5-10)\tau_0$ . In the second step (the slow step) the compound nucleus evaporates particles or goes into fission.

It is a well-known fact that fission is a slow process ( $\tau_f \sim 10^{-19}$  s) which occurs from an equilibrated nuclear system; this makes fission particularly valuable for studies of the target residues remaining after the preequilibrium emissions. Well-known also is the use of fission as a filter for studying reactions mechanisms (as recently reviewed by Viola<sup>3)</sup>) — in this paper we explore such possibility.

In this regard, electro- and photofission of preactinide nuclei are very convenient because of the following reasons:

- (1) as mentioned above, the primary process (photoexcitation) is well understood;
- (2) the photon can transfer substantial amounts of energy to the nucleus, but with comparatively small transfer of linear and angular momenta, which allows the observation of excitation energy effects *alone* (as evidenced in this work);
- (3) as nuclear matter is very transparent to photons, the whole nuclear volume is probed in a photoexcitation process. For example, pion photoproduction would occur, in

principle, with equal probability in all nucleons of the nucleus, with these nucleons acting as pion radiators.

(4) differently from what is verified for actinide (where fission barriers are  $\sim 6$  MeV), the fissility of preactinides (where fission barriers are of the order of 20–30 MeV) is a strong function of the excitation energy, which, by its turn, reflects peculiarities of the nuclear thermalization process (details below).

The electrofission of the preactinide nuclei  $^{208}\text{Pb}$  and  $^{209}\text{Bi}$  has been recently investigated in our Laboratory<sup>4,5)</sup>. A clear inflexion for  $^{208}\text{Pb}$ , and a less pronounced one for  $^{209}\text{Bi}$ , were observed in the electrofission cross section curves around 200–220 MeV. These findings were tentatively interpreted as being due to the behavior of the photopions inside the nucleus as revealed by their mean free path. Although appealing, the results for  $^{208}\text{Pb}$  and  $^{209}\text{Bi}$  cry for more experiments and, particularly, with emphasis in the energy region around 200–220 MeV.

Recently, Lucherini and collaborators<sup>6)</sup> measured in Frascati the photofission cross section of Au with quasimonochromatic photons, in the energy range of 120–300 MeV. Because of the quasimonochromatic nature of the photons, a photofission yield curve (integrated over the photon spectra) is obtained. It is interesting to note that this photofission yield seems to exhibit a shoulder at 220–230 MeV but, because of the overall fluctuation of the data points in this region, its statistical significance is questionable.

In this paper we present results for the electrofission cross section of the preactinides Au and Ta; the energy region around the supposed inflexions ( $\sim 200$ –220 MeV) was carefully measured at intervals of 5 MeV. A simple visual inspection of the cross section curves, for both Au and Ta, reveals the presence of inflexions similar to those observed for  $^{208}\text{Pb}$  and  $^{209}\text{Bi}$ . By means of an original data analysis and interpretation, we show, for the first time, that these inflexions are related to the nuclear thermalization process at its stage of preequilibrium emissions.

## II. THEORETICAL ASPECTS

Structures in the photofission cross section  $\sigma_{\gamma,f}$  manifest themselves as inflexions in the corresponding electrofission cross section curve  $\sigma_{e,f} = \sigma_{e,f}(E_e)$  because, by the virtual-photon theory,

$$\sigma_{e,f}(E_e) = \int_0^{E_e} \sigma_{\gamma,f}(\omega) N^{E1}(\omega, E_e) \frac{d\omega}{\omega}, \quad (1)$$

where  $N^{E1}$  is the  $E1$ -virtual-photon spectrum,  $\omega$  is the real (or virtual) photon energy, and  $E_e$  is the incident electron energy. We justify below why only the  $E1$ -virtual-photon spectrum is considered.

As discussed in the *Introduction*, the photofission of heavy nuclei following absorption of intermediate energy photons proceeds by means of a two-step process, where a compound nucleus ( $A_{CN}, Z_{CN}$ ) with excitation energy  $E_x$  undergoes fission. However, for a given photon energy  $\omega$ ,  $E_x$  exhibits a distribution in the interval  $0-\omega$  (see Fig. 1); thus, we propose to express the  $(\gamma, f)$  cross section, related to a specific compound nucleus, as

$$\sigma_{\gamma,f}(A_{CN}, Z_{CN}; \omega) = \sum_i N(E_{x_i}, \omega) \sigma_{CN}(A_{CN}, Z_{CN}; E_{x_i}, \omega) P_f(A_{CN}, Z_{CN}; E_{x_i}), \quad (2)$$

where  $P_f$  is the fission probability,  $\sigma_{CN}$  is the cross section for compound nucleus formation, and  $N(E_x, \omega)$  is the probability of finding a compound nucleus with excitation energy equal to  $E_x$ . In this regard, Guaraldo and collaborators<sup>7,8)</sup> performed detailed calculations based on the intranuclear cascade model (as described in Ref. 7) and obtained  $E_x$ -distributions  $N(E_x, \omega)$  in several nuclei, for photon energies between 100 and 300 MeV — these distributions are represented by histograms centered at  $E_x$ , (Fig. 1). Then, the sum in eqn. 2 runs for all the histograms comprised in the energy interval  $0-\omega$ .

Since, in principle, several compound nuclei could be formed after the preequilibrium emissions, the experimentally obtained photofission cross section is given by

$$\sigma_{\gamma,f}(\omega) = \sum_{A_{CN}, Z_{CN}} \sigma_{\gamma,f}(A_{CN}, Z_{CN}; \omega) \quad (3)$$

In the photon energy range pertinent to this paper, the  $A_{CN}$  and  $Z_{CN}$ -distributions are not broad. In fact, at  $\omega = 220$  MeV for  $^{197}\text{Au}$  we have<sup>7)</sup>

$$\Delta A_{CN} = A_t - \bar{A}_{CN} \cong 1.5, \quad \text{and} \quad (4)$$

$$\Delta Z_{CN} = Z_t - \bar{Z}_{CN} \cong 0.5, \quad (5)$$

where  $A_t$  and  $Z_t$  refer to the target nucleus. Thus, we can simplify our theoretical approach by assuming that *only one* compound nucleus ( $\bar{A}_{CN}, \bar{Z}_{CN}$ ), a “mean compound nucleus”, is formed.

Also, we note that  $\sigma_{\gamma,f}(\omega)$ , eqns. 2 and 3, depends explicitly on  $\sigma_{CN}$ , which is a quantity not available experimentally. So, it is necessary to express  $\sigma_{CN}$  in terms of a well-known quantity as e.g. the photoabsorption cross section  $\sigma_{\gamma,a}(\omega)$ . This was achieved by adopting, to the photonuclear reactions, a formalism developed by Kikuchi and Kawai<sup>9)</sup> plus our “mean compound nucleus” assumption (details on the calculations will be published soon<sup>10)</sup>), resulting in the following relationship

$$\frac{\sigma_{CN}(E_x)}{E_x} = \frac{\sigma_{\gamma,a}(\omega)}{\omega}, \quad \text{with} \quad E_x = E_x(\omega) \quad (6)$$

Substituting eqn. 6 in eqn. 2 we obtain

$$\sigma_{\gamma,f}(\omega) = \frac{\sigma_{\gamma,a}(\omega)}{\omega} \sum_i N(E_{x_i}, \omega) E_{x_i} P_f(\bar{A}_{CN}, \bar{Z}_{CN}; E_{x_i}) \quad (7)$$

This last result contains all the required physical quantities necessary for the data interpretation in this work. We note in passing that at  $\omega \lesssim 180$  MeV the  $E_x$ -distributions are nearly symmetric; then, if we substitute  $E_x$  by  $\bar{E}_x$  in eqn. 7,

$$\sigma_{\gamma,f}(\omega) \simeq \sigma_{\gamma,a}(\omega) \frac{\bar{E}_x}{\omega} \sum_i N(E_{x_i}, \omega) P_f(E_{x_i}), \quad (8)$$

where  $\bar{E}_x/\omega$  is approximately constant for  $\omega \lesssim 180$  MeV<sup>7</sup>). Therefore, the “effective”  $(\gamma, f)$ -fissility is proportional to some sort of mean-weighted of the compound nucleus fission probability,  $\sum_i N(E_{x_i}, \omega) P_f(E_{x_i})$ .

Since at energies below the peak of the delta resonance ( $\sim 300$  MeV)  $\sigma_{\gamma,a}$  is a structureless function of  $\omega$ , it is quite obvious that possible structures in the  $(\gamma, f)$  cross section are generated by the “mean-weighted- $P_f$ ”. However, the fission probability of a preactinide nucleus is a smooth and steep rising function (nearly exponential) of  $E_x$  (see table VII-1 of Ref. 11); thus, only “distortions” in the distributions  $N(E_x, \omega)$  could explain a drastic change in the slope of the  $(\gamma, f)$  curve, as reported in the present work for Au and Ta.

Finally, we note that at lower energies ( $\omega \lesssim 50$  MeV),  $E_x \cong \omega$  and, since  $\sum_i N = 1$ , our derived expression for  $\sigma_{\gamma,f}$  (eqn. 7) becomes trivially  $\sigma_{\gamma,f}(\omega) = \sigma_{\gamma,a}(\omega) P_f(\omega)$ .

### III. EXPERIMENT AND RESULTS

In view of the facts and reasonings cited above, we decided to perform a careful and detailed measurement of the electrofission cross section of Au and Ta. The difficulties associated with possible  $(e, e'f)$  exclusive measurements of preactinide nuclei have been pointed out elsewhere<sup>12</sup>); typical single-armed fission cross sections range from  $10^{-3}$  to 1 microbarn. If coincidence is imposed, the  $(e, e'f)$  cross sections become several orders of magnitude lower than that of  $(e, f)$ , which makes these experiments very time consuming.

Targets of Au and Ta with high purity were irradiated with electron beams from the Tohoku University linear accelerator, with energies from 40 to 250 MeV in steps of 5 and 10 MeV. Mica foils were used as fission fragment detectors, and the electron beam

was monitored by means of a ferrite core monitor. Details about the procedures and experimental set up were published elsewhere<sup>4</sup>).

In Fig. 2 is shown our electrofission for Au and Ta in the energy interval 180–250 MeV, which corresponds to the energy region where the searched out inflexions are located. The data points in the full range, 40–250 MeV, were used for a better delineation of the unfolded  $(\gamma, f)$  curve (details below).

We would like to stress the following points:

(1) the reproducibility of the  $(e, f)$  experimental points is around 5–10%, so that the inflexions exhibited in Fig. 2 are not artifacts of the experimental fluctuations.

(2) the  $(e, f)$  curves of preactinides are steep functions of the energy, which makes the presence of inflexions and shoulders much more evident. For actinides the situation is opposite, because their fissilities saturates (around 100%) for energies above 50 MeV; as a consequence, the  $(e, f)$  curves are very flat and, therefore, do not respond accordingly to changes in  $E_x$ .

(3) the remarkable similarity between the Au and Ta  $(e, f)$  curves demonstrates the physical significance of the inflexions. We would say that the independently obtained Au and Ta curves are “twin curves” in a normalized scale, despite the fact that their absolute values differ by nearly one order of magnitude. Therefore, each one of these nuclei works as a *veto* to the other. In this sense, an observed inflexion is accepted as a “physical fact” (and not a fluctuation) only if it is observed in *both nuclei* at the same energy position. The physical nature of the inflexions, shown in Fig. 2, is considerably reinforced by the occurrence of similar inflexions in <sup>209</sup>Bi and <sup>208</sup>Pb (see Fig. 3 of Ref. 5).

### IV. DATA INTERPRETATION

As discussed above, the inflexions in the  $(e, f)$  curves correspond to structures in the  $(\gamma, f)$  cross section curves (see Eqn. 1). Thus, we can say that a mere visual inspection of

Fig. 2 allows a qualitative delineation of the  $(\gamma, f)$  structures. However, for the delineation of the magnitude of the  $(\gamma, f)$  cross section, we need to perform the unfolding of the  $(e, f)$  integrated cross section.

#### IV-A. UNFOLDING PROCEDURE

We used a least structure unfolding routine developed at our Laboratory<sup>4)</sup>, where the experimental data are fitted with a continuous curve; this curve is input in a subroutine which performs matrix inversion and introduces a smoothing parameter. By varying this parameter, within a previously determined interval, a set of solutions is obtained. Next, each solution is folded-back and compared with the experimental data; in this procedure a chi-square is calculated. The accepted solution is the one who provided the closest to total chi-square. The "smoothing criterion" of the unfolding routine works in such a way that, a structure arising from an isolate statistical fluctuation of two adjacent data points is smoothed out. Thus, only the structure delineated by several consecutive data points, in a wider energy interval, resists to the smoothing.

We performed the unfolding using only  $E1$ -virtual-photon spectra, calculated in the DWBA with the inclusion of nuclear size effects<sup>13)</sup>, because of the following reasons.

Part of the total photoabsorption cross section above the photopion threshold ( $\sim 140$  MeV) corresponds to the quasi-deuteron absorption mechanism, while another part refers to photopion production. The former consists mostly of  $E1$ -excitations, and the latter is usually parametrized in  $M1$  and  $E1$  parts (as described in Refs. 14 and 15); we represent them by  $\sigma_{QD}$ ,  $\sigma_{\pi}(M1)$ , and  $\sigma_{\pi}(E1)$ , respectively. Therefore, the general expression for the  $(e, f)$  cross section is given by

$$\sigma_{e,f}(E_e) = \int_0^{E_e} \left[ \sigma_{QD}(\omega) P_f(E1; \omega) N^{E1}(\omega, E_e) + \sigma_{\pi}(M1; \omega) P_f(M1; \omega) N^{M1}(\omega, E_e) + \sigma_{\pi}(E1; \omega) P_f(E1; \omega) N^{E1}(\omega, E_e) \right] \frac{d\omega}{\omega} \quad (9)$$

In the electron energy range of our experiment, the shapes and intensities of the  $E1$ ,  $M1$  and  $E2$  virtual-photon spectra (VPS) become very similar, at least for  $\omega > \frac{1}{2} E_e$ <sup>13,16)</sup>. We show in Fig. 3 the  $E1$  and  $M1$  VPS for electrons of 240 MeV scattered by Au, plus the photofission cross section of Au. We note that the  $(\gamma, f)$  cross section below  $\sim 120$  MeV ( $\frac{1}{2} E_e$ ) is nearly two orders of magnitude lower, comparatively to  $\omega > 120$  MeV. Therefore, the contribution from  $\omega < 120$  MeV to the integrated  $(e, f)$  cross section is small; thus, in our approach we can assume that  $N^{E1} \cong N^{M1}$ , without incurring in errors greater than 3%.

In addition, at excitation energies well above the fission barrier, the nuclear level densities of states populated in  $E1$ ,  $E2$ , and  $M1$  photoexcitation processes have the same magnitude; thus, it is quite reasonable to assume, under statistical grounds, that

$$P_f(E2) \cong P_f(E1) \cong P_f(M1) \quad ,$$

as pointed out in Ref. 17 (and references therein).

So, Eqn. 9 can be rewritten as

$$\sigma_{e,f}(E_e) \cong \int_0^{E_e} [\sigma_{QD}(\omega) + \sigma_{\pi}(M1; \omega) + \sigma_{\pi}(E1; \omega)] P_f(\omega) N^{E1}(\omega, E_e) \frac{d\omega}{\omega} \quad , \quad (10)$$

where  $\sigma_{QD} + \sigma_{\pi}(M1) + \sigma_{\pi}(E1)$  is the total photoabsorption cross section  $\sigma_{\gamma,a}$  and, as a consequence, the unfolded quantity is  $\sigma_{\gamma,a} P_f$  (the photofission cross section  $\sigma_{\gamma,f}$ ).

The fact that  $N^{E1} \cong N^{M1} \cong N^{E2}$ , at intermediate energies, makes electrofission (and electrodisintegration) cross sections rather insensitive to the relative strengths of the multipoles involved (also discussed in Ref. 18). Although this renders difficult to obtain information on the multipole composition (which is not the goal of this work), it does give confidence that the shapes of the unfolded cross sections (based on  $E1$  only) are reasonably reliable. Magnitudes are reliable too, as we demonstrated through the

comparison of the unfolded  $(\gamma, f)$  cross section of  $^{209}\text{Bi}$  with that obtained in Frascati using quasi-monochromatic photons (see Fig. 3 of Ref. 4).

Also shown in Fig. 2 is the unfolded  $(\gamma, f)$  cross section  $\sigma_{\gamma, f}$  of Au (that for Ta is very similar); the uncertainty band of the unfolded curve (not drawn in Fig. 2) is  $\sim 15\%$ .

#### IV-B. THERMALIZATION RELATED EFFECT

It is quite evident the occurrence of a  $(\gamma, f)$ -shoulder at 200–220 MeV (Fig. 2), which cannot be explained in terms of discontinuities neither in  $\sigma_{\gamma, a}$  nor in  $P_f$ . As discussed in Section II, possible structures in  $\sigma_{\gamma, f}$  could be explained only by some sort of distortion in the  $E_x$ -distribution function  $N(E_x, \omega)$ , which changes the slope of the “mean-weighted- $P_f$ ” ( $\langle P_f \rangle$ ) (see Eqns. 7 and 8).

In this regard we note that for  $\omega \lesssim 180$  MeV the  $E_x$ -distribution is practically symmetric around the average value  $\bar{E}_x = \frac{1}{2}\omega$ , while for  $\omega > 200$  MeV  $N(E_x, \omega)$  becomes very wide, close to a Maxwell distribution, with a maximum around  $E_x = 20$ –40 MeV (Fig. 1, and Refs. 7 and 8). However, at photon energies around 200 MeV we observe a splitting in the  $E_x$ -distributions into two well separate structures at  $E_x \approx 25$  and 105 MeV. Without going over to any detailed calculations, we observe that the presence of a “high-energy component” in  $N(E_x, \omega)$ , at  $E_x \approx 105$  MeV, where  $P_f$  is much higher relatively to  $E_x \approx 25$  MeV, gives rise to a quite enhanced  $\langle P_f \rangle$ . Since at  $\omega \gtrsim 220$  MeV the  $E_x$ -distributions assume low-energy peaked Maxwellian shapes, it becomes clear that a change in the slope of  $\sigma_{\gamma, f}(\omega)$  takes place at  $\omega \approx 200$ –220 MeV, as experimentally observed.

Besides this qualitative verification, we calculated the  $(\gamma, f)$  cross section for Au using the expression deduced in this work (Eqn. 7), plus the  $E_x$ -distributions calculated elsewhere<sup>7,8)</sup>, at photon energies from 180 to 260 MeV; also, we took published values for  $\sigma_{\gamma, a}(\omega)$ <sup>19)</sup>. The fission probability of the mean compound nucleus (see Section II) was

calculated by means of well-known statistical based relations<sup>11,17)</sup> and procedures<sup>17)</sup>, plus the assumption that the level density is described by the so-called Fermi gas expression<sup>11)</sup>. Since at  $E_x \geq 30$  MeV shell effects in nuclei are absent<sup>20)</sup>, we used liquid-drop quantities calculated by the method of Myers and Swiatecki<sup>21)</sup>, in order to obtain fission barriers and neutron binding energies of all nuclei participating in the fission-chain decay (Ref. 7 for more details). The result is shown in Fig. 2; the reproduction of the  $(\gamma, f)$ -shoulder, at 200–220 MeV, is striking within the 15% uncertainty band of the  $(\gamma, f)$  unfolded curve, and particularly if we consider the fact that our calculations have no free adjustable parameter.

As a check of the sensitiveness of the  $E_x$ -distributions in the delineation of the  $(\gamma, f)$ -shoulder, we repeated the calculation of  $\sigma_{\gamma, f}(\omega)$  at  $\omega = 200$  MeV using a function  $N(E_x, \omega)$  with a Maxwellian shape, similar to that at  $\omega \gtrsim 220$  MeV; in other words, we simply removed the high-energy component (at  $E_x \approx 105$  MeV) of  $N(E_x, \omega = 200$  MeV), but we kept the same area under this function. Now, the new  $\sigma_{\gamma, f}$  is lowered by a factor of two eliminating, therefore, the shoulder (see the dotted curve in Fig. 2).

It is worth remembering that the function  $N(E_x, \omega)$  is determined by the pre-equilibrium emissions of the thermalization process, that is, the magnitude and the shape of the  $E_x$ -distribution of the compound nucleus, depend on the *number* and *energy* of the particles (mostly protons and neutrons) emitted in the preequilibrium stage. This stage, by its turn, is governed by the intranuclear cascade process. Therefore,  $N(E_x, \omega)$  contains the peculiarities of the nuclear thermalization process. Since the very existence of the  $(\gamma, f)$ -shoulder is dictated by both the overall  $E_x$ -distribution and their fine details (e.g. the “splitting”), as shown by our calculations, we conclude that we have been recognized, for the first time, a thermalization related effect in the fission of Au and Ta. Similar structures previously observed in  $^{209}\text{Bi}$  and  $^{208}\text{Pb}$ <sup>4,5)</sup> are certainly associated to this same effect.

#### IV-C. THERMALIZATION versus PHOTOEXCITATION

Although photopion production is the competing photoexcitation mechanism with quasideuteron for  $\omega > 140$  MeV, its effectiveness in heating up the nucleus starts at  $\omega \gtrsim 200$  MeV. In fact, below this energy pions are photoproduced with kinetic energies  $T_\pi < 60$  MeV; in this energy range, the pion mean free path in the nuclear matter is  $\lambda_\pi \gtrsim 7$  fm<sup>22)</sup> (of the order of the nuclear radius) and, therefore, has a high probability of escaping from the nucleus — as a consequence, small energies are deposited. Thus, quasideuteron absorption is the leading mechanism to excite the nucleus for  $\omega \lesssim 200$  MeV.

Up to  $\omega \approx 160$ -180 MeV the  $E_x$ -distributions are practically symmetric around  $E_x \simeq \frac{1}{2}\omega$ ; as discussed above, this is the energy region where quasideuteron photoexcitation dominates.

For  $\omega \gtrsim 220$  MeV, the photoproduced pions have  $T_\pi \gtrsim 80$  MeV, corresponding to  $\lambda_\pi \lesssim 2$  fm<sup>22)</sup>, and are reabsorbed by a pair of nucleons, sharing their rest and kinetic energies. The two interacting nucleons acquire an energy of approximately  $\frac{1}{2}\omega$  each (since  $\omega \cong T_\pi + m_\pi$ , neglecting recoil); before leaving the nucleus these two nucleons lose a small fraction of their energy in inelastic scattering with other nucleons. This is quite understandable since for nucleons with energies  $\gtrsim 100$  MeV their mean free paths inside a nucleus are  $\gtrsim 6$ -7 fm<sup>23)</sup> (of the order of the nuclear radius). Thus, from the initial photon energy only a small fraction is converted into excitation energy explaining, therefore, the low-energy maximum in the  $N(E_x, \omega)$  functions at  $E_x \simeq 20$ -40 MeV, which is the common feature at  $\omega > 200$  MeV. The broad shape of these distribution functions indicates the occurrence of dispersion effects among the cascade nucleons and the rescattered photopions (before reabsorption).

Under the scenario pictured above, it becomes clear why the  $E_x$ -distributions around  $\omega = 200$  MeV exhibit two maxima. At this energy region there is a change in the nuclear excitation regime, from the dominance of the quasideuteron to that of photopion

production. As some sort of "transition region", characteristics of both processes coexist: the peak at  $E_x \approx \frac{1}{2}\omega$ , due to the quasideuteron process, and the low-energy peak attributed to the onset of the photopion production (as an effective mechanism for the heating up of the nucleus).

Therefore, the competition between the photoexcitation mechanisms determines the peculiarities of the thermalization process which, by its turn, reveals itself in the energy dependence of the photofission cross section, as demonstrated in the present work.

#### IV-D. POSSIBLE FISSION RELATED STRUCTURES

Our calculations of  $\sigma_{\gamma,f}$ , which explain the  $(\gamma, f)$ -shoulders experimentally observed for Au and Ta, rely on the assumption that these nuclei decay statistically by fission; this gives rise to fission probabilities strongly increasing with  $E_x$ . We would like to discuss the correctness of this assumption.

The fission probability would decrease for an increasing  $E_x$ , if substantially less fissionable residual systems are formed; in such a circumstance, a fission related structure could appear in the  $(\gamma, f)$  cross section. In fact, the so-called "saturation effects" in the fission probability are likely to manifest above  $E_x = 100$ -200 MeV, where preequilibrium emission of heavy fragments (the nuclear fragmentation), and/or the fast nucleon cascade, leads to residual systems that are too light, and/or too cold, to fission (we refer the reader to Ref. 24 for a very detailed discussion on this issue).

However, in the photon energy range of the present work ( $\omega \leq 250$  MeV), the mean excitation energies are  $\lesssim 85$  MeV<sup>7,8)</sup>. Therefore, a significant slowing down of the fission process, comparatively to expectations based on the statistical model, is unlikely.



## V. CONCLUDING REMARKS

(1) The results from this work for Au and Ta, plus those previously obtained for  $^{209}\text{Bi}$  and  $^{208}\text{Pb}$ <sup>4,5</sup>, constitute a considerable body of evidences supporting the physical nature of the  $(e, f)$ -inflexions around 200–220 MeV.

(2) The corresponding  $(\gamma, f)$ -structures (or shoulders), associated to these  $(e, f)$ -inflexions, are nicely described as a direct consequence of fine thermalization related effects around  $\omega = 200$  MeV, which dictate the shape characteristics of the  $E_x$ -distribution functions  $N(E_x, \omega)$ .

(3) It is shown that the peculiar shape of  $N(E_x, \omega)$  at  $\omega = 200$  MeV (double-peaked distribution) is due to an interplay between the two leading photoexcitation mechanisms: quasideuteron and pion photoproduction. In this regard, the role played by the photopion mean free path inside the nucleus is addressed.

(4) Finally, an original formalism for the analysis of photofission at intermediate energies is worked out.

We would like to thank Dr. V. Lucherini and Dr. E. De Sanctis, for providing us with their complete set of results for  $E_x$ -distributions. Thanks are also due to the Linac crew for providing the specified electron beam.

This work was partially supported by Conselho Nacional de Desenvolvimento Científico e Tecnológico (Brazil) and Japan Society for the Promotion of Science.

## REFERENCES

- (1) V.E. Bunakov, *Part. Nucl.* **11** (1980) 1285.
- (2) A.S. Iljinov, M.V. Mebel, C. Guaraldo, V. Lucherini, E. De Sanctis, N. Bianchi, P. Levi Sandri, V. Muccifora, E. Polli, A.R. Reolon, P. Rossi, and S. Lo Nigro, *Phys. Rev.* **C39** (1989) 1420.
- (3) V.E. Viola, *Nucl. Phys.* **A502** (1989) 531c.
- (4) J.D.T. Arruda-Neto, M. Sugawara, T. Tamae, O. Sasaki, H. Ogino, H. Miyase, and K. Abe, *Phys. Rev.* **C34** (1986) 935.
- (5) J.D.T. Arruda-Neto, M. Sugawara, H. Miyase, T. Kobayashi, T. Tamae, K. Abe, M. Nomura, H. Matsuyama, H. Kawahara, K. Namai, M.L. Yoneama, and S. Siminonatto, *Phys. Rev.* **C41** (1990) 354.
- (6) V. Lucherini, C. Guaraldo, E. De Sanctis, P. Levi Sandri, E. Polli, A.R. Reolon, A.S. Iljinov, S. Lo Nigro, S. Aiello, V. Bellini, V. Emma, C. Milone, G.S. Pappalardo, and M.V. Mebel, *Phys. Rev.* **C39** (1989) 911.
- (7) C. Guaraldo, V. Lucherini, E. De Sanctis, A.S. Iljinov, M.V. Mebel, and S. Lo Nigro, *Il Nuovo Cimento* **103A** (1990) 607.
- (8) V. Lucherini, private communication.
- (9) K. Kikuchi and M. Kawai: "Nuclear Matter and Nuclear Reactions", North-Holland (Amsterdam), 1968, p. 244.
- (10) J.D.T. Arruda-Neto, A. Deppman, N. Bianchi, E. De Sanctis, A. Fantoni, P. Levi Sandri, V. Lucherini, V. Muccifora, E. Polli, A.R. Reolon, P. Rossi, A.J. Iljinov, and M.V. Mebel, *Nucl. Phys. A* (to be submitted).
- (11) R. Vandenbosch and J.R. Huizenga: "Nuclear Fission", Academic (New York), 1973, p. 232, 254, 255.

- (12) J.D.T. Arruda-Neto, M. Sugawara, H. Miyase, T. Kobayashi, T. Tamae, K. Abe, M. Nomura, H. Matsuyama, H. Kawahara, K. Namai, M.L. Yoneama, and S. Siminonatto, *J. Phys. G* **15** (1989) L215.
- (13) F. Zamani-Noor and D.S. Onley, *Phys. Rev. C* **33** (1986) 1354.
- (14) B. Ziegler, *Lecture Notes in Physics* **108**, ed. H. Arenhövel and D. Drechsel (Springer, Berlin, 1979) p. 148.
- (15) K.P. Schelhaas, J.M. Henneberg, M. Sanzone-Arenhövel, N. Wieloch-Laufenberg, U. Zurmühl, B. Ziegler, M. Schumacher, and F. Wolf, *Nucl. Phys. A* **489** (1988) 189.
- (16) P. Durgapal and D.S. Onley, *Phys. Rev. C* **27** (1983) 523.
- (17) H. Dias, J.D.T. Arruda-Neto, B. Carlson, and M. Hussein, *Phys. Rev. C* **39** (1989) 564.
- (18) G.J. Miller, J.C. McGeorge, I. Anthony, R.O. Owens, and D. Ryckbosch, *Nucl. Phys. A* **551** (1993) 135.
- (19) A. Leprêtre, P. Carlos, H. Beil, R. Bergère, J. Fagot, A. De Miniac, and A. Veysière, *Nucl. Phys. A* **431** (1984) 573.
- (20) E.A. Cherepanov, A.S. Iljinov, and M.V. Mebel, *J. Phys. G* **9** (1983) 1397.
- (21) W.D. Myers and W.J. Swiatecki, *Ark. Fyz.* **36** (1986) 343.
- (22) A.M. Bernstein, in "Photopion Nuclear Physics", edited by P. Stoler (Plenum, New York, 1979), p. 406.
- (23) R.D. McKeown, S.J. Sanders, J.P. Schiffer, H.E. Jackson, M. Paul, J.R. Specht, E.J. Stephenson, R.P. Redwine, and R.E. Segel, *Phys. Rev. Lett.* **44** (1980) 1033.
- (24) Th. Blaich, M. Begemann-Blaich, M.M. Fowler, J.B. Wilhelmy, H.C. Britt, D.J. Fields, L.F. Hansen, M.N. Namboodiri, T.C. Sangster, and Z. Fraenkel, *Phys. Rev. C* **45** (1992) 689.

## FIGURE CAPTIONS

**Fig. 1** —  $E_x$ -distribution functions  $N(E_x, \omega)$  of the compound nuclei produced in the photoexcitation of Au, for  $\omega = 160, 200$  and  $240$  MeV. All histograms refer to Monte Carlo intranuclear-cascade calculations, from Refs. 7 and 8.

**Fig. 2** — Electrofission cross section of Au (left-hand scale) and Ta (right-hand scale); the dashed curves are to guide the eyes. The solid curve is the unfolded photofission cross section of Au (in arbitrary unit) — the uncertainty, not shown, is  $\sim 15\%$ . The curves represented by  $\times$ — $\times$  and  $\dots\dots$  are the calculated photofission cross section of Au (details in the text).

**Fig. 3** —  $E1$  and  $M1$  virtual-photon spectra of  $^{197}\text{Au}$ , for electrons of  $240$  MeV, calculated in the DWBA with nuclear size-effects included<sup>13</sup> (left-hand scale), and the unfolded photofission cross section of  $^{197}\text{Au}$  (right-hand scale).

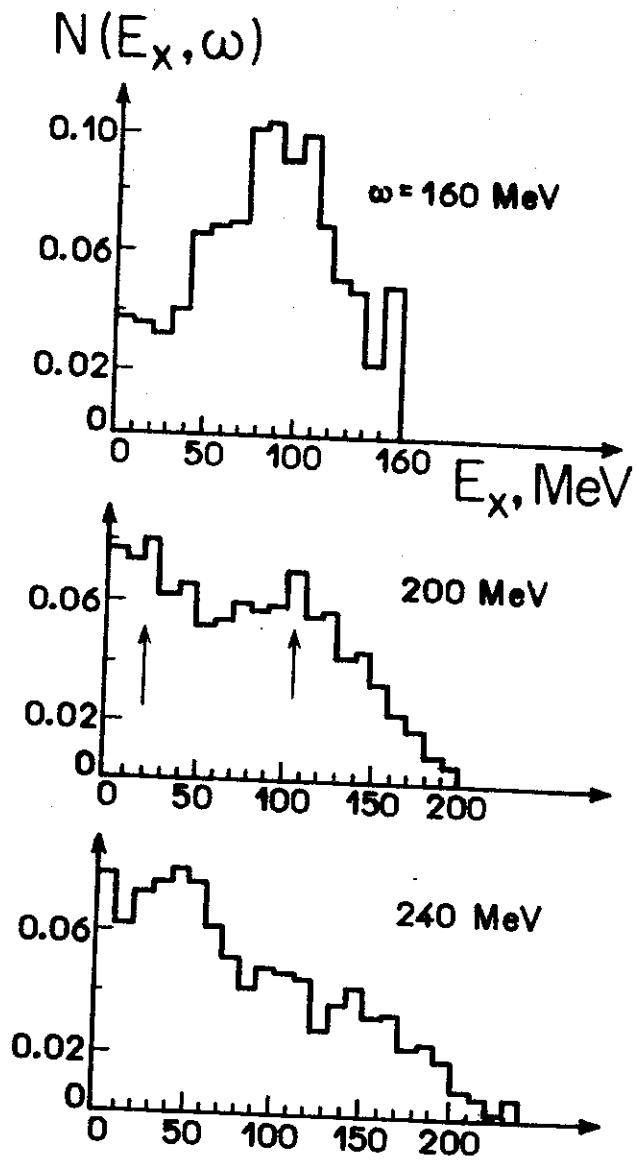
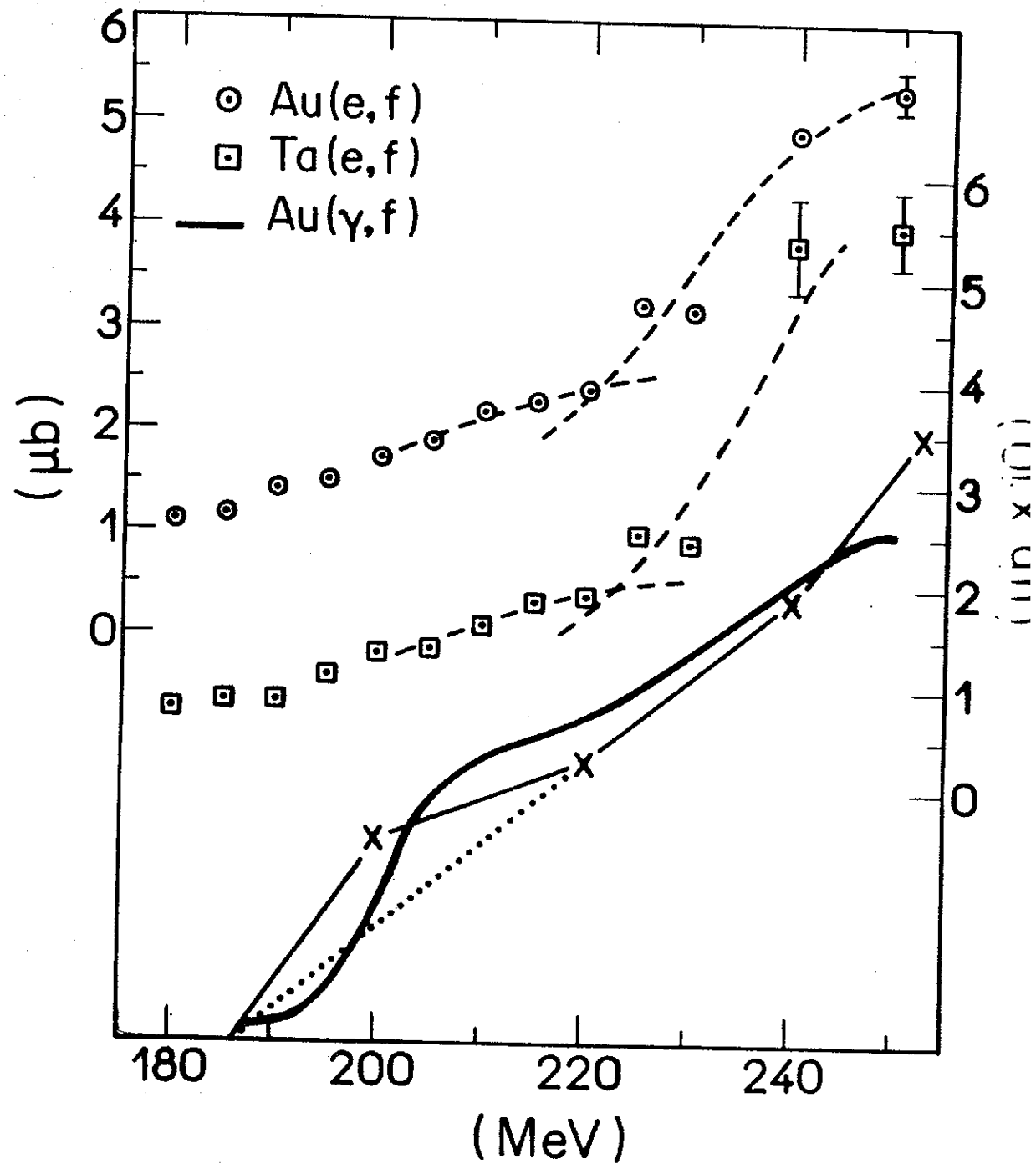


Fig. 1



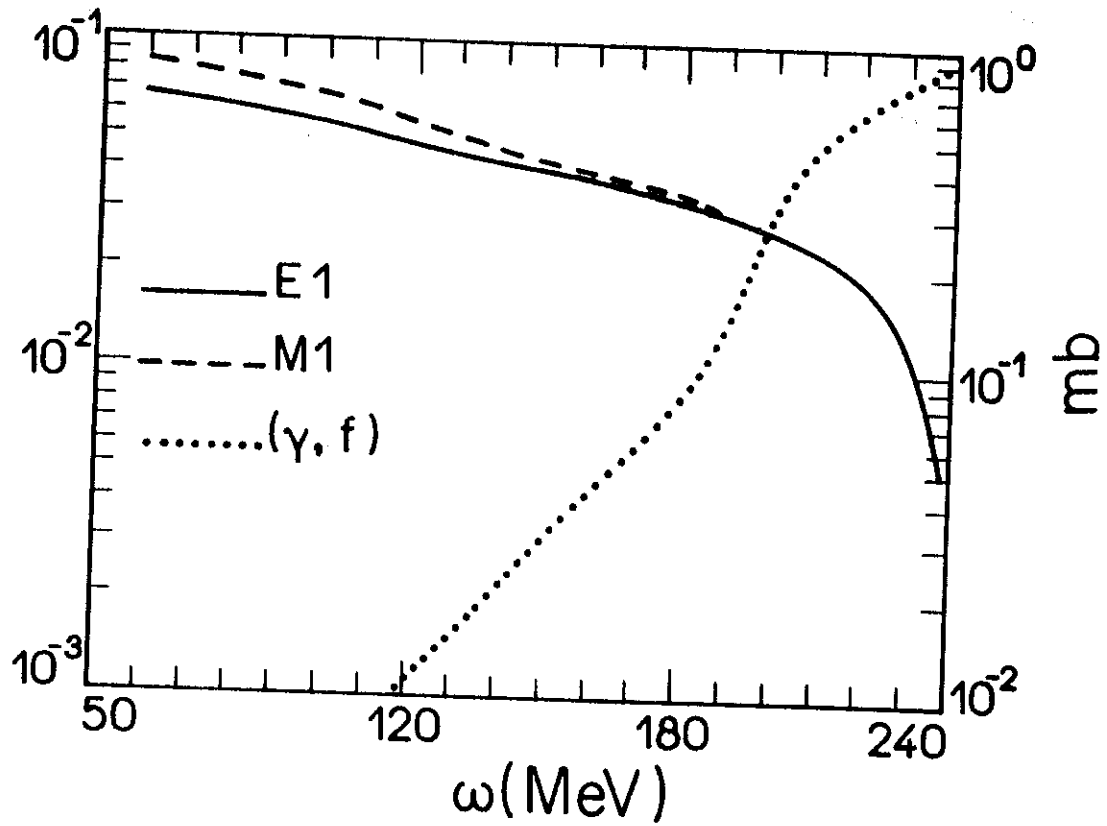


Fig. 3